

UC Davis

UC Davis Previously Published Works

Title

Histone deacetylase inhibitors synergizes with catalytic inhibitors of EZH2 to exhibit anti-tumor activity in small cell carcinoma of the ovary, hypercalcemic type

Permalink

<https://escholarship.org/uc/item/19c5h12r>

Journal

Molecular Cancer Therapeutics, 17(12)

ISSN

1535-7163

Authors

Wang, Yemin
Chen, Shary Yuting
Colborne, Shane
[et al.](#)

Publication Date

2018-12-01

DOI

10.1158/1535-7163.mct-18-0348

Peer reviewed



Published in final edited form as:

Mol Cancer Ther. 2018 December ; 17(12): 2767–2779. doi:10.1158/1535-7163.MCT-18-0348.

Histone deacetylase inhibitors synergizes with catalytic inhibitors of EZH2 to exhibit anti-tumor activity in small cell carcinoma of the ovary, hypercalcemic type

Yemin Wang^{1,2,*}, Shary Yuting Chen^{1,2}, Shane Colborne³, Galen Lambert², Chae Young Shin², Nancy Dos Santos⁴, Krystal A. Orlando⁵, Jessica D. Lang⁶, William P.D. Hendricks⁶, Marcel B. Bally⁴, Anthony N. Karnezis^{1,2}, Ralf Hass⁷, T. Michael Underhill⁸, Gregg B. Morin^{3,9}, Jeffrey M. Trent⁶, Bernard E. Weissman⁵, and David G. Huntsman^{1,2,10,*}

¹Department of Pathology and Laboratory Medicine, University of British Columbia, Vancouver, BC, Canada

²Department of Molecular Oncology, British Columbia Cancer Research Centre, Vancouver, BC, Canada

³Michael Smith Genome Science Centre, British Columbia Cancer Agency, Vancouver, BC, Canada

⁴Department of Experimental Therapeutics, British Columbia Cancer Research Centre, Vancouver, BC, Canada

⁵Department of Pathology and Laboratory Medicine and Lineberger Comprehensive Cancer Center, University of North Carolina, Chapel Hill, NC, USA

⁶Division of Integrated Cancer Genomics, Translational Genomics Research Institute (TGen), Phoenix, AZ, USA

⁷Department of Obstetrics and Gynecology, Hannover Medical School, D-30625 Hannover, Germany

⁸Department of Cellular and Physiological Sciences and Biomedical Research Centre, University of British Columbia, Vancouver, BC, Canada

⁹Department of Medical Genetics, University of British Columbia, Vancouver, BC, Canada

¹⁰Department of Obstetrics and Gynaecology, University of British Columbia, Vancouver, BC, Canada

Abstract

Small cell carcinoma of the ovary, hypercalcemic type (SCCOHT) is a rare but extremely lethal malignancy that mainly impacts young women. SCCOHT is characterized by a diploid genome

*Correspondence to: Yemin Wang, PhD., Department of Pathology and Lab Medicine, University of British Columbia 2660 Oak street, Vancouver, BC, V6H3Z6, Canada Phone: 1-604.875.4111 ext 21753; yewang@bccrc.ca and David Huntsman, MD, FRCPC, FCCMG, Dr. Chew Wei Memorial Professor of Gynaecologic Oncology, UBC, Professor, Departments of Pathology and Lab Medicine and Obstetrics and Gynaecology, UBC, Distinguished Scientist, Department of Molecular Oncology, BC Cancer Research Centre, 4111-675 West 10th Avenue, Vancouver, BC V5Z 1L3 Canada. Phone: 1-604.675.8205; dhuntsma@bccancer.bc.ca.

Conflict of interest: The authors declare no potential conflicts of interest.

with loss of SMARCA4 and lack of SMARCA2 expression, two mutually exclusive ATPases of the SWI/SNF chromatin-remodeling complex. We and others have identified the histone methyltransferase EZH2 as a promising therapeutic target for SCCOHT, suggesting that SCCOHT cells depend on the alternation of epigenetic pathways for survival. In this study, we found that SCCOHT cells were more sensitive to pan-HDAC inhibitors compared to other ovarian cancer lines or immortalized cell lines tested. Pan-HDAC inhibitors, such as quisinostat, reversed the expression of a group of proteins that were deregulated in SCCOHT cells due to SMARCA4 loss, leading to growth arrest, apoptosis and differentiation *in vitro* and suppressed tumor growth of xenografted tumors of SCCOHT cells. Moreover, combined treatment of HDAC inhibitors and EZH2 inhibitors at sub-lethal doses synergistically induced histone H3K27 acetylation and target gene expression, leading to rapid induction of apoptosis and growth suppression of SCCOHT cells and xenografted tumors. Therefore, our preclinical study highlighted the therapeutic potential of combined treatment of HDAC inhibitors with EZH2 catalytic inhibitors to treat SCCOHT.

Keywords

SCCOHT; SWI/SNF; chromatin-remodeling complex; differentiation; HDAC; EZH2; SMARCA4; ovarian cancer

Introduction

Small cell carcinoma of the ovary, hypercalcemic type (SCCOHT) is a rare type of ovarian cancer type with poorly differentiated histology, which primarily affects young women with a median age of diagnosis in mid-twenties (1–5). Unlike most common ovarian malignancies, the genome of SCCOHT is diploid with inactivating mutations of the *SMARCA4* gene, encoding the ATPase of the SWI/SNF chromatin-remodelling complex, as the only recurrent feature and the likely driver event in the majority of SCCOHT tumors (6–9). In addition, SCCOHT do not express SMARCA2 (10,11), the alternative ATPase of SWI/SNF chromatin-remodelling complex, a surprising finding given the requirement for SMARCA2 for the survival of most other SMARCA4-deficient cancer cells (12,13).

Despite the receipt of extensive chemotherapy following surgical debulking, the prognosis of SCCOHT patients is very poor with a 2-year survival rate less than 35% (14,15), highlighting the urgent demand to develop novel therapeutic options for these patients. Preclinical studies suggest that a subset of SCCOHT patients may benefit from c-Met inhibitors (16) or oncolytic virus (17). In concordance with the known antagonism between SWI/SNF complex and the polycomb repressive complex 2 (PRC2), we and Chan-Penebre et al. have both recently demonstrated that SCCOHT cells are highly sensitive to catalytic inhibition of EZH2, the enzymatic subunit of the PRC2 complex (18,19). Despite the therapeutic promise of targeting the epigenome of SCCOHT, clinical trial testing of the EZH2 inhibitor EPZ-6438 (tazemetostat) only led to stable disease or partial response in two SCCOHT patients, previously treated with chemotherapy (www.epizyme.com). Therefore, determining whether SCCOHT cells depend on additional epigenetic modulators for survival and whether targeting them can improve the response of SCCOHT cells to EZH2 inhibition remains a priority.

Through regulating the acetylation state of histones, histone deacetylases (HDACs) and acetyltransferases play important roles in the maintenance of chromatin and in regulating many biological processes including transcriptional control, chromatin plasticity, protein-DNA interactions and cell differentiation, growth and death (20–22). Dozens of HDAC inhibitors, targeting one or several HDACs, have been developed as anticancer agents for reversing aberrant epigenetic states associated with cancer. Most of them induce apoptosis and cell cycle arrest and prevent invasion, metastasis and angiogenesis. Several pan-HDAC inhibitors, such as SAHA (vorinostat), romidepsin and panobinostat, have been approved by the US FDA for treating various hematopoietic malignancies, such as cutaneous T-cell lymphoma. However, treatment with HDAC inhibitors as single agents has often demonstrated limited clinical benefit for patients with solid tumors, prompting the investigation of genetic vulnerability associated with HDAC inhibition and treatment combinations with other cancer therapeutics to improve their clinical utility.

Herein, we demonstrate that that SCCOHT cells were more sensitive to HDAC inhibitors compared to other ovarian cancer lines. While HDAC inhibitors induced apoptosis and differentiation of SCCOHT cells, the combined treatment with EZH2 inhibitors synergistically suppressed their proliferation, triggered apoptosis and inhibited their tumor growth in xenograft models.

Materials and methods

Cell culture and chemicals

Cells were cultured in either DMEM/F-12 (BIN67, SCCOHT-1, COV434 and SVOG3e) or RPMI (all other lines) supplemented with 10% FBS and maintained at 37 °C in a humidified 5% CO₂-containing incubator. All cell lines have been certified by STR analysis, tested regularly for *Mycoplasma* and used for the study within six months of thawing. EPZ-6438 (23), quisinostat (24), SAHA, romidepsin and panobinostat were purchased from Selleckchem for *in vitro* studies. EPZ-6438 and quisinostat were purchased from Active Biochemku for *in vivo* studies.

Plasmids, siRNAs and lentivirus packaging

Lenti-GFP (EX-EGFP-Lv102) and Lenti-SMARCA4 (EX-Y4637-Lv102) plasmids were obtained from Genecopeia (EX-Y4637-Lv102). A SMARCA2 gRNA targeting the SMARCA2 genomic region (5'-CTTGTCATGTATAACCATCGATGG-3') was cloned into lentiCRISPR vector (Addgene #49535) to construct lentiCRISPR-SMARCA2. Specific siRNAs used to knock down HDAC1 were purchased from Dharmacon, including D-003493-04 (#1) and D-003493-09 (#2). Specific siRNAs used to knock down HDAC2, 5'-GCUACUAAGAUGUGCAAAGAAGACA-3' (#1) and 5'-CCAGAACACUCCAGAAUAUAUGGAA-3' (#2), were obtained from Integrated DNA Technology. To produce lentivirus expressing SMARCA4 gene or SMARCA2 gRNA, Lenti-SMARCA4 or LentiCRISPR-SMARCA2 was co-transfected with packaging plasmids psPAX2 and pMD2.G into HEK293T cells. Supernatants were collected at 48 and 72 h for lentivirus preparation and infection.

Cell viability assay

Cells were seeded in 96-well plates in quadruplicate at a density of 500–2000 cells per well depending on the growth curve of each cell line. Twenty-four hours later, cells were treated with either DMSO or HDAC inhibitors at indicated 9 doses (decreasing in two-fold dilution from the highest concentration). For drug combination assays, cells were treated with HDAC inhibitors (i.e. quisinostat, 0–6 nM) and EZH2 inhibitors (i.e. EPZ-6438, 0–1 μ M) at various ratios. Six days after treatment, cells were fixed in methanol:acetic acid:water solution (1:1:8) and then stained with 0.5% crystal violet in methanol. The absorbed dye was resolubilized with 10% acetic acid and measured spectrophotometrically at 595 nM. Cell survival was calculated by normalizing the absorbance to that of DMSO-treated controls.

Epigenetic drug library screen

Cells seeded in 96-well plates were exposed to epigenetic drug library (Cayman #11076) at 1 μ M. After six days, cells were fixed and proceeded to cell viability measurement as described above. Three independent assays were performed to calculate the average cell growth inhibition rate, determined by (100-%cell remaining of drug-treated well)/%survival of cell remaining of DMSO-treated wells.

Clonogenic assay

Cells were seeded in 6-well (SCCOHT-1, 2000 cells/well) or 12-well plates (BIN67: 1000 cells/well; COV434: 250 cells/well) in triplicate. Twenty-four hours later, cells were treated with either DMSO or 2 nM quisinostat. Drugs were refreshed every 4–5 days. Two weeks after treatment, cells were fixed in 10% methanol-10% acetic acid and then stained with 0.5% crystal violet to determine the numbers of colonies under each condition.

Spheroid growth assay

To determine the effect of quisinostat on spheroid formation, SCCOHT cells were mixed in culture media containing 3% matrigel and then seeded into 6-well plates pre-coated with matrigel. DMSO or quisinostat were then added in media with 3% matrigel and refreshed every 3–4 days. For analyzing the effect of quisinostat on pre-formed spheroids, cells (2000 cells/well) were seeded in 200 μ l medium per well containing 2% Matrigel (Corning) in 96-well plates pre-coated with 1% agarose. After being centrifuged at 1000xg for 5 minutes, cells were cultured for three days to allow formation of spheroids. Then, culture medium was changed together with adding either DMSO or Quisinostat at indicated dose. After being exposed to drug for 6-days, cell viability was measured by CelltiterGlo (Promega) and normalized to DMSO-treated cells.

Cell cycle and apoptosis analysis

Cells treated with DMSO or quisinostat were fixed with 70% ice-cold ethanol, stained for DNA content with propidium iodide and subjected to flow cytometry analysis to quantitate cell cycle distribution. To monitor apoptosis, the cell-permeable dye (NucView™ 488 dye) coupled to an activated caspase-3/7 recognition motif (Essen Bioscience) was added to the culture medium of cells treated as indicated. Upon activation through cleavage by the activated caspase-3/7 during apoptosis, the dye was released and bound to DNA

fluorescently, which was detected using the IncuCyte live cell imaging system. The apoptotic index was calculated by dividing the overall fluorescent object counts by cell numbers under each condition.

Western blotting

Whole-cell extracts were obtained for SDS-PAGE electrophoresis as previously described (25). Primary antibodies used were rabbit anti-SMARCA4 (Abcam, ab110641), H3K27Me3 (Millipore, 07-449), Myc (Abcam, ab32072), mouse anti-EZH2 (BD Bioscience, 612667), vinculin (Sigma, v9264), Actin (Sigma, A5441), Histone H3 (Abcam, ab1791), MAP2 (Millipore, MAB3418), TUBB3 (Santa Cruz, sc-51670), BAD (Santa Cruz, sc-8044), p16 (Ventana, 725-4713) and CDKN1A/p21 (BD Pharmacogen, 556430) and horseradish peroxidase-conjugated anti-mouse and anti-rabbit IgG (Amersham). Chemiluminescence was used for detection (Perkin-Elmer Life Sciences). Actin or vinculin were used as protein loading controls.

Proteomics

Cells were lysed in 100mM HEPES buffer (pH 8.5) containing 1% SDS and 1x protease inhibitor cocktail (Roche). After chromatin degradation by benzonase, reduction and alkylation of disulfide bonds by dithiothreitol and iodoacetamide, samples were cleaned up and prepared for trypsin digestion using the SP3-CTP method (26). In brief, proteins were digested for 14 h at 37 °C followed by removal of SP3 beads. Tryptic peptides from each sample were individually labeled with TMT 10-plex labels, pooled and fractionated into 12 fractions by high pH RP-HPLC, desalted, orthogonally separated and analyzed using an Easy-nLC 1000 coupled to a Thermo Scientific Orbitrap Fusion mass spectrometer operating in MS3 mode. Raw MS data were processed and peptide sequences were elucidated using Sequest HT in Proteome Discoverer software (v2.1.0.62), searching against the UniProt Human Proteome database.

Mouse xenografts

All animal work procedures were performed according to institutional guidelines approved by the Animal Care Committee of the University of British Columbia (A14-0290). In brief, BIN67 or SCCOHT-1 cells (1×10^7 cells/mouse) were injected with a 1:1 mix of Matrigel (Corning) subcutaneously into the back of NRG (NOD.Rag1KO.IL2R γ CO) mice. Mice were randomized to treatment arms once the average tumor volume reached 100 mm^3 (BIN67) or 250 mm^3 (SCCOHT-1). Quisinostat was formulated in 20% hydroxypropyl- β -cyclodextrin (final pH 8.70) and administered intraperitoneally at 5, 10 or 20 mg/kg once daily (M/W/F) for three weeks. For drug combination, mice were dosed with 5 mg/kg quisinostat (M/W/F) and 200 mg/kg EPZ-6438 once daily (M-Sat, formulated in 0.5% NaCMC (Sigma) containing 0.1% Tween-80) alone or in combination for three weeks, followed by drug removal. Tumor size and mouse weight were measured twice or thrice weekly. Tumor volume was calculated as $\text{length} \times (\text{width})^2 \times 0.52$. For Quisinostat single drug efficacy studies, mice were terminated when reaching humane endpoint (i.e. tumor reaches 1000 mm^3) or at the end of 3-week treatment, whichever came first. For drug combination study, mice were terminated until reaching humane endpoint.

Statistical analysis

Student's *t*-test was used to evaluate the significant difference between two groups in all experiments except proteomics. The Peptide Expression Change Averaging (PECA) analysis (27) was performed for comparing the proteomic profiles of BIN67 cells treated with or without EPZ-6438 to generate signal log ratio values (log fold-change), *p*-values and false discovery rate (fdr) adjusted *p*-values (*p.fdr*) using peptide level signal values. The PECA analysis (27) was performed for comparing the proteomic profiles of BIN67 cells treated with or without EPZ-6438. Survival curves and IC₅₀ of drug treatment were determined by PRISM software or Microsoft Excel. The drug combination indexes were calculated using the Chou-Talalay method and CalcuSyn software (Biosoft, Cambridge, UK). A *p*-value or *p.fdr*-value (for proteomics data) < 0.05 was considered significant.

Results

Epigenetic drug screen identifies synthetic lethal targets in SCCOHT

The simplicity of SCCOHT genome suggests that the epigenetic rewiring, in response to defective SWI/SNF chromatin remodeling, may drive tumorigenesis of SCCOHT. To search for potential therapeutic agents that specifically target SCCOHT, we screened an epigenetic drug library that includes 62 compounds targeting various epigenetic modifiers in three SCCOHT cell lines (BIN67, SCCOHT-1 and COV434), two ovarian high-grade serous carcinoma cell lines (OVCAR-4 and ES-2) and an immortalized human granulosa cell line (SVOG3e) (Supplemental Table S1). We performed the screen at 1 μM to identify clinically relevant inhibitors for further studies. Although some of the compounds are not effective at this dose, two EZH2 catalytic inhibitors (EPZ-6438 and GSK126) significantly suppressed the growth of SCCOHT cells with little effects on other cell lines as we previously reported (19) (Fig. 1A and 1B), validating the selectivity of our screen. Notably, multiple histone deacetylase (HDAC) inhibitors displayed preferential suppression of the SCCOHT cells, including SAHA, a clinically used pan-HDAC inhibitor approved for cutaneous T-cell lymphoma (Fig. 1B, *P* < 0.01).

SCCOHT cells are sensitive to pan-HDAC inhibitors

Next, we validated the cellular response to HDAC inhibitors in three SCCOHT cell lines versus a subset of ovarian epithelial carcinoma cell lines. SAHA, panobinostat and quisinostat, the three pan-HDAC inhibitors in either clinic use or various trials, effectively suppressed the growth of three SCCOHT cell lines with IC₅₀s significantly lower than other ovarian cancer cell lines examined (Fig. 1C and Supplemental Fig. S1, *p*<0.01).

We focused on quisinostat, which has displayed promising results for refractory cutaneous T-cell lymphoma and solid malignancies in recent clinical trials (28,29) and induced histone H3 acetylation rapidly in all three SCCOHT cell lines (Fig. 1D). Treatment of quisinostat at sub-lethal doses suppressed SCCOHT cell growth in a time-dependent manner (Supplemental Fig. S2A) and inhibited their colony formation abilities significantly (Fig. 1E). Moreover, treatment of quisinostat completely blocked the formation of BIN67 spheroids at a sub-lethal dose (Fig. 1F) and dramatically suppressed the growth of pre-formed spheroids of three SCCOHT cell lines at higher concentration (Fig. 1G). As

quisinostat has minimal effect on HDAC6 activity (24), the hypersensitivity of SCCOHT cells to quisinostat can be attributed to inhibition of class I or other class II HDACs. Accordingly, depletion of HDAC1 or HDAC2 completely killed SCCOHT-1 cells and significantly reduced the proliferation of BIN67 cells (Supplemental Fig. S2B-S2D). Simultaneous knockdown of HDAC1 and HDAC2 exhibited significantly stronger inhibitory effect on the growth of BIN67 cells (Supplemental Fig. S2E). These data suggested that inhibition of HDACs, such as class I HDACs, may have therapeutic potential for SCCOHT patients.

To address whether SMARCA4 and SMARCA2 dual deficiency can predict the sensitivity to HDAC inhibitors in other cell contexts, we assessed the sensitivity of a panel of lung cancer cell lines with various states of SMARCA4 and SMARCA2 expression to HDAC inhibitors. All these cell lines, regardless of SMARCA4 and SMARCA2 status, responded similarly to either SAHA or quisinostat treatment with IC50s much higher than those of SCCOHT cell lines (Supplemental Fig. S3A and S3B). In addition, knockdown of SMARCA4 by shRNAs in MiaPaCa-2 cells, a pancreatic cancer cell line with no detectable SMARCA2 (30), did not increase the cellular sensitivity to HDAC inhibitors (Supplemental Fig. S3C-E). Therefore, the greater sensitivity of SCCOHT cells to HDAC inhibition appears to be cell context dependent.

Quisinostat induces cell cycle arrest, apoptosis and differentiation in SCCOHT cells

Concordant with growth suppression, BrdU incorporation was dramatically reduced by quisinostat treatment in a dose-dependent manner (Fig. 2A), suggesting that quisinostat inhibited the proliferation of SCCOHT cells. Next, we analyzed the effect of Quisinostat on cell cycle distribution and cell death. Low doses of quisinostat (5 nM) induced cell cycle arrest at G1 phase, whereas higher doses of quisinostat (20, 50 nM) significantly triggered cell death (sub-G1) in all three SCCOHT cell lines 72 hours post treatment (Fig. 2B). Using a fluorescence-based live cell imaging of activated caspase-3/7 activity, we further determined that quisinostat elicited apoptosis rapidly in dose- and time-dependent manners in SCCOHT cells (Fig. 2C).

The SCCOHT cells that survived the treatment of 50 nM quisinostat displayed a bipolar and elongated morphology (Fig. 2D). Prolonged treatment of quisinostat at a lower dose (10 nM) also induced morphology change, which largely resembled neurons after 3 weeks of treatment (Supplemental Fig. S4A). Similar morphology changes were observed in SCCOHT cells upon exposure to other HDAC inhibitors, such as SAHA and panobinostat (Supplemental Fig. S4B), suggesting that HDAC inhibition triggers the differentiation of SCCOHT cells.

Effect of quisinostat on the proteome of SCCOHT cells

To elucidate the molecular mechanisms underlying the cellular response of SCCOHT cells to quisinostat, we performed proteomic analysis of BIN67 cells treated with vehicle or 10 nM quisinostat for 24 hours or 72 hours using mass spectrometry. Proteomics analysis revealed that 5.9% (402/6819) and 16.4% (1115/6819) of the BIN67 proteome was significantly altered by at least two folds upon quisinostat treatment for 24 or 72 hours,

respectively (Fig. 3A, Supplemental Table S2-S4, **p.fdr<0.05**) (Fig. 3B). In agreement with the potent growth suppression by quisinostat treatment, Ingenuity Pathway analysis (IPA) revealed a significant enrichment of genes involved in cell cycle control and cell death (Supplemental Table S5 and Fig. 3C). Quisinostat treatment significantly increased the levels of CDKN1A, a cyclin-dependent kinase inhibitor required for cell cycle arrest by HDAC inhibition (31) ($\text{Log}_2\text{FC}=2.0$ and 2.0), and the pro-apoptotic protein Bak1 ($\text{Log}_2\text{FC}=0.5$ and 1.58) in a time-dependent manner. The expression of c-Myc, a key cell cycle player under the direct control by SWI/SNF chromatin remodeling complex (32), was suppressed in a time-dependent manner ($\text{Log}_2\text{FC}=-1.5$ and -1.7). Immunoblotting confirmed these findings and revealed a significant induction of cleaved PARP (Fig. 3E and 3F), supporting the induction of growth arrest and apoptosis upon quisinostat treatment. Furthermore, in line with the morphology change after quisinostat treatment (Fig. 2D), IPA predicted that the biological processes called “development of neurons” and “morphogenesis of neurons” were activated 72 hours following quisinostat treatment (Fig. 3D). Supporting this, quisinostat treatment induced the expression of MAP2 ($\text{Log}_2\text{FC}=0.54$ and 1.39) and TUBB3 ($\text{Log}_2\text{FC}=1.15$ and 1.85), two markers of neuronal cells, and reduced EZH2 levels in a time-dependent manner (Fig. 3F). Moreover, several biological processes known to play important roles in neuron development, such as organization of cytoskeleton, microtubule dynamics and formation of cellular protrusions, cell migration and endocytosis, all appeared as activated in the presence of quisinostat in a time-dependent manner (Fig. 3D, Supplemental Table S5). These observations suggest that quisinostat elicited neuronal-like differentiation in SCCOHT cells.

Consistent with our previous observation (10), the levels of SMARCA2 protein and mRNA was induced by quisinostat in a time-dependent manner (Supplemental Table S5, $\text{log}_2\text{FC}=2.6$ and 3.2 ; Fig. 3F and Supplemental Fig. S5A). To address whether SMARCA2 induction was important for the cellular sensitivity to quisinostat, we employed CRISPR/cas9 technology to deplete SMARCA2, which prevented the induction of SMARCA2 upon quisinostat treatment in COV434 cells (Supplemental Fig. S5B). This minimally made COV434 cells more resistant to quisinostat (Supplemental Fig. S5C), suggesting only a small contribution of SMARCA2 induction in the cellular sensitivity of SCCOHT cells to quisinostat.

SMARCA4 and HDAC co-regulate the genes involved in cell fate decision

To gain more insights into the cellular hypersensitivity of SCCOHT cells to HDAC inhibitors, we determined whether HDAC inhibition activated genes that were deregulated by SMARCA4 inactivation. First, we profiled the proteomes of BIN67 cells with ectopic expression of either GFP or SMARCA4. About 5.6% (370/6604) and 1.3% (86/6604) of the identified proteins were significantly upregulated or downregulated, respectively, by at least two folds upon SMARCA4 re-expression in BIN67 cells (Fig. 4A, Supplemental Table S6, **p.fdr<0.05**). Pathway analysis of the significantly altered proteins by IPA revealed an enrichment of proteins involved in several molecular and cellular functions, such as cellular movement, cellular assembly and organization and cell death with a few biological processes being predicted to be activated or inhibited, such as the activation of neuron-like development (Fig. 4B, Supplemental Table S7), which was supported by the altered cell

morphology (Fig. 4C). Next, we compared the proteins altered by either quisinostat treatment (72 hour) or SMARCA4 re-expression (96 hours after infection) ($|\text{Log}_2\text{FC}| \geq 1$, $p, \text{fdr} < 0.05$). A subset of proteins (194 upregulated, 62 down-regulated) was altered by both SMARCA4 re-expression and quisinostat treatment (Fig. 4D, Supplemental Table S8), many of which contributed to induction of cell death, inhibition of cell progression or the development of a neuronal phenotype and related biological processes as predicted by IPA (Fig. 4E, Supplemental Table S9). These results suggest that loss of SMARCA4 in the unknown precursor cell of SCCOHT may render them dependent on the activity of HDACs for resistance to cell death signals and maintenance of their poorly differentiated state and oncogenic properties.

Quisinostat suppressed the growth of SCCOHT mouse xenograft

To further investigate the efficacy of quisinostat *in vivo*, we tested the potency of quisinostat in xenograft models of SCCOHT. In the BIN67 xenograft model, treatment of quisinostat at either 10 or 20 mg/kg once daily for three weeks (M/W/F) was generally well tolerated without body weight loss (Supplemental Fig. S6A). Tumor growth was rapidly and effectively suppressed by either 10 or 20 mg/kg quisinostat (Fig. 5A). The final average tumor weight was also dramatically reduced in quisinostat-treated groups in comparison to the vehicle-treated group after three weeks (Fig. 5B, $p < 0.001$ and $p < 0.01$). Western blotting analysis confirmed that the acetylation of histone H3, but not tubulin, was induced by the treatment of either dose of quisinostat and the expression of c-Myc was also significantly reduced in a dose-dependent manner in quisinostat-treated cells (Fig. 5C). However, xenografted tumors expressed substantial amount of CDKN1A that did not differ between vehicle and quisinostat-treated groups, indicating that a significant portion of cells in xenografted tumors may undergo growth arrest after substantial growth and/or other cell populations residing in the tumor may undergo arrest with upregulated CDKN1A expression. As SCCOHT-1 cells were significantly more sensitive to quisinostat than BIN67 cells *in vitro* (Supplemental Fig. S1), we further tested the effect of 5 mg/Kg quisinostat (M/W/F) on the growth of SCCOHT-1 xenograft tumors, which was significantly reduced by the treatment (Fig. 5D). However, all quisinostat-treated SCCOHT-1 tumors progressed during the 3-week treatment period with the median survival time to humane endpoint being increased from 6.5 days to 13 days upon treatment (Fig. 5E, $P = 0.001$), implying that 5mg/Kg of quisinostat, which is comparable to the recommended dose for human (28,29), can significantly, but not completely, suppress SCCOHT tumor growth.

Synergism between HDAC and EZH2 inhibitors in SWI/SNF deficiency-driven tumors

We and others have previously demonstrated that SCCOHT cells are hypersensitive to the pharmacological inhibition of PRC2 complex with EZH2 inhibitors (18,19). It has also been reported that HDACs are recruited by the PRC2 complex to the regulatory regions of PRC2 targets, where they act in concert to silence the expression of their targets (33). Therefore, we determined whether simultaneous inhibition of both HDAC and EZH2 might synergize to inhibit the cell growth. Combined treatment of quisinostat and EPZ-6438 synergistically suppressed cell growth in a wide range of dose combinations in SCCOHT cells (Fig. 6A and Supplemental Fig. S7A) and other SWI/SNF-deficient cells, such as TOV112D (a SCCOHT-like cell line) (18), G401 (a malignant rhabdoid tumor cell line) and SYO-1 cells (a synovial

sarcoma cell line) (Supplemental Fig. S7B-D) and triggered apoptosis rapidly in BIN67 and COV434 cells than treatment with either drug alone (Fig. 6B). Furthermore, depletion of HDAC2 significantly increased the sensitivity of BIN67 cells to EPZ-6438 treatment (Supplemental Fig. S8), whereas combination of quisinostat and GSK126 or combination of EPZ-6438 and panobinostat or romidepsin (a Class I HDAC inhibitor) also synergistically suppressed the growth of SCCOHT cells (Supplemental Fig. S9), suggesting that the synergism was not an off-target effect of quisinostat and EPZ-6438 combination.

Next, we determined the levels of global histone H3K27Me3 and H3K27Ac in SCCOHT cells treated with EPZ-6438 and quisinostat alone or in combination by western blotting. As shown in Fig. 6C, the level of histone H3K27Me3 was effectively reduced by EPZ-6438, but not quisinostat. Treatment with either quisinostat or EPZ-6438 increased H3K27Ac, while combined treatment of quisinostat and EPZ-6438 elicited higher levels of H3K27Ac than either drug alone, suggesting a more profound effect on the activation of their targets. Consequently, a robust induction of CDKN1A (p21) was observed when SCCOHT cells were exposed to both drugs simultaneously (Fig.6C).

Lastly, we determined the efficacy of combined treatment of EPZ-6438 and quisinostat in the BIN67-xenograft model. In agreement with our previous finding (19), daily single dose treatment of EPZ-6438 at 200 mg/Kg failed to suppress BIN67 xenografted tumor growth, while 5 mg/Kg quisinostat (once daily, M/W/F) only mildly suppressed tumor growth ($p < 0.05$). Combination of EPZ-6438 and quisinostat completely blocked the growth of tumor (Fig. 6D, $p < 0.001$) with only a mildly increased mouse body weight loss compared to single treatment of either drugs (Supplemental Fig. S10A). Upon removal of the drug following three weeks of treatment, tumors that received combinational treatment started to grow after a short delay with the tumor volume doubling time not significantly different with the tumors in the vehicle-treated group, suggesting that a longer treatment period may be required to fully defeat the tumor growth. The median survival time of the tumor-bearing mice was greatly improved from 44.5 days in vehicle group to 70 days in the group received combinational treatment (Supplemental Fig. S10B, $p < 0.001$).

Discussion

SCCOHT is a rare but extremely lethal malignancy of the ovary. There is an urgent demand for effective therapeutic agents to treat patients with SCCOHT. Through a rationale epigenetic drug screen, we identified that pan-HDAC inhibitors, a class of anti-cancer drugs that regulate gene expression through interrupting the deacetylation of histones and non-histone proteins, have preferential growth suppressive effects in SCCOHT cells. As our screen is performed at a single but clinically relevant dose (1 μM), we cannot rule out epigenetic modifiers other than HDAC and EZH2 may be putative targets in SCCOHT cells because some of the tool compounds in the library is not effective at 1 μM (Supplemental Table S1). Although a few HDAC inhibitors have been approved for clinical management of several types of hematopoietic tumors, their efficacy in solid malignancies remains unresolved. Our present study demonstrates that pan-HDAC inhibitors displayed a significantly higher preclinical potency in SCCOHT cells than in other ovarian cancer cell lines. Importantly, the IC50s of quisinostat (~ 2 nM) in SCCOHT cell is on the lower end of

the reported C_{max} (0.87–3.44 ng/ml, equivalent to 2.2–8.7 nM) in patients who received 12 mg quisinostat, the recommended dosage for phase 2 clinical trials (29). Furthermore, combined treatment of either pan-HDAC inhibitors or a class I HDAC inhibitor with EZH2 catalytic inhibitors, which were previously reported by us and others to kill SCCOHT cells selectively (18,19), displayed a robust synergistic effect in growth suppression of SCCOHT cells and xenograft tumors. Therefore, we have provided preclinical evidence that SCCOHT patients may benefit from the treatment of pan-HDAC inhibitors alone or in combination with EZH2 inhibitors.

HDAC inhibitors have been reported to regulate various cellular functions, such as cell proliferation, cell death, DNA repair and differentiation (34). Accordingly, quisinostat, a hydroxamic acid derivative and second generation pan-HDAC inhibitor (24), caused cell cycle arrest, activated differentiation and induced apoptosis in SCCOHT cells. Proteomic analysis further validated that quisinostat regulated the expression of proteins involved in cell cycle arrest, death and neuronal differentiation. Importantly, a subset of these proteins were also regulated by re-expression of SMARCA4 in SCCOHT cells, suggesting that HDAC inhibitors can revert the expression of genes dysregulated by SWI/SNF remodeling complex deficiency in SCCOHT. Interestingly, HDAC inhibitors have been reported to be effective in malignant rhabdoid tumor models and activate the genes that are deregulated due to SMARCB1 loss (35). Therefore, the SWI/SNF complex may be functionally antagonistic to HDACs, in addition to the PRC2 complex (19,36). Intriguingly, PRC2 complex can also recruit HDACs, via EED, to repress targets transcriptionally (33). Therefore, cancer cells with a deficient SWI/SNF complex will likely rely on the activity of PRC2 and HDAC complex that act in concert to suppress the genes required for differentiation and tumor suppression. This notion is further strengthened by our observation that simultaneous inhibition of HDAC and EZH2 displayed a stronger effect on the acetylation of histone H3K27 globally and the expression of target genes than treatment with either agent alone and elicited a robust synergistic effect in the suppression of SCCOHT cells. Future analysis of the histone acetylation status in the promoter or enhancer regions of those genes upon HDAC inhibitor treatment or restoration of the functional SWI/SNF complex will improve our understanding of the antagonism between SWI/SNF complex and HDAC.

Although SCCOHT cells were highly sensitive to HDAC inhibitors, we did not detect significant difference in the cellular responses to HDAC inhibitors among lung cancer cell lines with loss of SMARCA4 and/or SMARCA2 expression. Depletion of SMARCA4 in a SMARCA2-deficient pancreatic cancer cell line also had little effect on cellular sensitivity to HDAC inhibitors. Thus, the dual deficiency of SMARCA4 and SMARCA2 cannot predict the cellular response to HDAC inhibitors, similar as what was observed for EZH2 inhibitors (19). These results suggest that the high burden of genetic mutations in common malignancies may abrogate their selective sensitivity to epigenetic targeting even in the absence of a functional SWI/SNF complex. Future studies to identify targets that can sensitize cancer cells to EZH2 or HDAC inhibitors may help to improve the efficacy of epigenetic therapy in common malignancies.

The synergistic interaction between EZH2 depletion and HDAC inhibitors has been reported in several cancer types, such as human acute myeloid leukemia, gallbladder carcinoma, and

non-small cell lung cancer cells (37–39). However, depletion of EZH2 will affect the non-catalytic function of EZH2 warranting further evaluation of its clinical safety. Our present study for the first time demonstrates that combined suppression of EZH2 catalytic activity and HDACs in a wide range of dose combinations has a synergistic effect in SCCOHT preclinical models without significant adverse events. This synergism is likely due to upregulated transcription as a result of hyperacetylation of H3K27 at the promoter or enhancer of PRC2 targets by simultaneous inhibition of EZH2 and HDAC, and/or hyperacetylation of histone lysine residues by HDAC in addition to increased acetylation of H3K27. Moreover, our finding of the synergism of combined treatment of HDAC inhibitors and EZH2 catalytic inhibitors also holds the promise beyond SCCOHT. TOV112D, a SCCOHT-like cell line with SMARCA4/SMARCA2 dual deficiency and great sensitivity to EZH2 inhibition (18), displayed a strong response to HDAC inhibitors alone or in combination with EZH2 inhibitors. A robust synergistic effect between HDAC and EZH2 inhibitor was also detected in G401 cells, a malignant rhabdoid tumor cell line with high sensitivity to HDAC inhibition (35) or EZH2 inhibition (40), and SYO-1 cells, a synovial carcinoma cell line with SWI/SNF complex deficiency caused by SS18-SSX fusion and great response to quisinostat (41). Therefore, the combinational therapy of EZH2 and HDAC inhibitors may provide a putative therapeutic approach for treating patients with poorly differentiated tumors driven primarily by the loss of activity of the SWI/SNF chromatin remodeling complex, such as SCCOHT, dedifferentiated endometrial carcinoma, rhabdoid tumors, synovial sarcoma, epithelioid sarcoma and undifferentiated thoracic sarcomas (42–45).

Supplementary Material

Refer to Web version on PubMed Central for supplementary material.

Acknowledgements

We acknowledge the technical support of Sarah Maines-Bandiera, Winnie Yang, Ashley Wang, Nicole Wretham, Dana Masin, Hong Yan, Jenna Rawji and Chris Ke-dong Wang. We thank Drs. Barbara Vanderhyden, Mikko Anttonen and Torsten Nielsen for providing BIN67, COV434 and SYO-1 cells, respectively. This work was supported by research funds from the Canadian Cancer Society Research Institute (#703458, to D.G. Huntsman, Y. Wang, M. Bally and A.N. Karnezis), the National Cancer Institute of NIH (United States) (1R01CA195670–01, to D.G. Huntsman, J.M. Trent and B.E. Weissman), the Terry Fox Research Institute Initiative New Frontiers Program in Cancer (TFF1021, to D.G. Huntsman), the British Columbia Cancer Foundation (to D.G. Huntsman), the VGH & UBC Hospital Foundation (to D.G. Huntsman).

Reference:

1. Longy M, Toulouse C, Mage P, Chauvergne J, Trojani M. Familial cluster of ovarian small cell carcinoma: a new mendelian entity? *J Med Genet* 1996;33(4):333–5. [PubMed: 8730291]
2. Martinez-Borges AR, Petty JK, Hurt G, Stribling JT, Press JZ, Castellino SM. Familial small cell carcinoma of the ovary. *Pediatr Blood Cancer* 2009;53(7):1334–6 doi 10.1002/pbc.22184. [PubMed: 19621450]
3. Florell SR, Bruggers CS, Matlak M, Young RH, Lowichik A. Ovarian small cell carcinoma of the hypercalcaemic type in a 14 month old: the youngest reported case. *Med Pediatr Oncol* 1999;32(4):304–7. [PubMed: 10102028]
4. Estel R, Hackethal A, Kalder M, Munstedt K. Small cell carcinoma of the ovary of the hypercalcaemic type: an analysis of clinical and prognostic aspects of a rare disease on the basis of

- cases published in the literature. *Arch Gynecol Obstet* 2011;284(5):1277–82 doi 10.1007/s00404-011-1846-5. [PubMed: 21298438]
5. Young RH, Oliva E, Scully RE. Small cell carcinoma of the ovary, hypercalcemic type. A clinicopathological analysis of 150 cases. *Am J Surg Pathol* 1994;18(11):1102–16. [PubMed: 7943531]
 6. Ramos P, Karnezis AN, Craig DW, Sekulic A, Russell ML, Hendricks WP, et al. Small cell carcinoma of the ovary, hypercalcemic type, displays frequent inactivating germline and somatic mutations in SMARCA4. *Nat Genet* 2014;46(5):427–9 doi 10.1038/ng.2928. [PubMed: 24658001]
 7. Kupryjanczyk J, Dansonka-Mieszkowska A, Moes-Sosnowska J, Plisiecka-Halasa J, Szafron L, Podgorska A, et al. Ovarian small cell carcinoma of hypercalcemic type - evidence of germline origin and SMARCA4 gene inactivation. a pilot study. *Pol J Pathol* 2013;64(4):238–46. [PubMed: 24375037]
 8. Witkowski L, Carrot-Zhang J, Albrecht S, Fahiminiya S, Hamel N, Tomiak E, et al. Germline and somatic SMARCA4 mutations characterize small cell carcinoma of the ovary, hypercalcemic type. *Nat Genet* 2014;46(5):438–43 doi 10.1038/ng.2931. [PubMed: 24658002]
 9. Jelinic P, Mueller JJ, Olvera N, Dao F, Scott SN, Shah R, et al. Recurrent SMARCA4 mutations in small cell carcinoma of the ovary. *Nat Genet* 2014;46(5):424–6 doi 10.1038/ng.2922. [PubMed: 24658004]
 10. Karnezis AN, Wang Y, Ramos P, Hendricks WP, Oliva E, D'Angelo E, et al. Dual loss of the SWI/SNF complex ATPases SMARCA4/BRG1 and SMARCA2/BRM is highly sensitive and specific for small cell carcinoma of the ovary, hypercalcaemic type. *J Pathol* 2016;238(3):389–400 doi 10.1002/path.4633. [PubMed: 26356327]
 11. Jelinic P, Schlappe BA, Conlon N, Tseng J, Olvera N, Dao F, et al. Concomitant loss of SMARCA2 and SMARCA4 expression in small cell carcinoma of the ovary, hypercalcemic type. *Mod Pathol* 2016;29(1):60–6 doi 10.1038/modpathol.2015.129. [PubMed: 26564006]
 12. Hoffman GR, Rahal R, Buxton F, Xiang K, McAllister G, Frias E, et al. Functional epigenetics approach identifies BRM/SMARCA2 as a critical synthetic lethal target in BRG1-deficient cancers. *Proc Natl Acad Sci U S A* 2014;111(8):3128–33 doi 10.1073/pnas.1316793111. [PubMed: 24520176]
 13. Wilson BG, Helming KC, Wang X, Kim Y, Vazquez F, Jagani Z, et al. Residual complexes containing SMARCA2 (BRM) underlie the oncogenic drive of SMARCA4 (BRG1) mutation. *Mol Cell Biol* 2014;34(6):1136–44 doi 10.1128/MCB.01372-13. [PubMed: 24421395]
 14. Clement PB. Selected miscellaneous ovarian lesions: small cell carcinomas, mesothelial lesions, mesenchymal and mixed neoplasms, and non-neoplastic lesions. *Mod Pathol* 2005;18 Suppl 2:S113–29 doi 10.1038/modpathol.3800313. [PubMed: 15492757]
 15. Robert H Young EO, Robert E Scully. Small Cell Carcinoma of the Ovary, Hypercalcemic Type. *The American Journal of Surgical Pathology* 1994;18(11):1102–16. [PubMed: 7943531]
 16. Otte A, Rauprich F, von der Ohe J, Yang Y, Kommos F, Feuerhake F, et al. c-Met inhibitors attenuate tumor growth of small cell hypercalcemic ovarian carcinoma (SCCOHT) populations. *Oncotarget* 2015;6(31):31640–58 doi 10.18632/oncotarget.5151. [PubMed: 26436697]
 17. Gamwell LF, Gambaro K, Merzotis M, Crane C, Arcand SL, Bourada V, et al. Small cell ovarian carcinoma: genomic stability and responsiveness to therapeutics. *Orphanet J Rare Dis* 2013;8:33 doi 10.1186/1750-1172-8-33. [PubMed: 23433318]
 18. Chan-Penebre E, Armstrong K, Drew A, Grassian AR, Feldman I, Knutson SK, et al. Selective Killing of SMARCA2- and SMARCA4-deficient Small Cell Carcinoma of the Ovary, Hypercalcemic Type Cells by Inhibition of EZH2: In Vitro and In Vivo Preclinical Models. *Mol Cancer Ther* 2017;16(5):850–60 doi 10.1158/1535-7163.MCT-16-0678. [PubMed: 28292935]
 19. Wang Y, Chen SY, Karnezis AN, Colborne S, Santos ND, Lang JD, et al. The histone methyltransferase EZH2 is a therapeutic target in small cell carcinoma of the ovary, hypercalcaemic type. *J Pathol* 2017;242(3):371–83 doi 10.1002/path.4912. [PubMed: 28444909]
 20. Barneda-Zahonero B, Parra M. Histone deacetylases and cancer. *Mol Oncol* 2012;6(6):579–89 doi 10.1016/j.molonc.2012.07.003. [PubMed: 22963873]
 21. Witt O, Deubzer HE, Milde T, Oehme I. HDAC family: What are the cancer relevant targets? *Cancer Lett* 2009;277(1):8–21 doi 10.1016/j.canlet.2008.08.016. [PubMed: 18824292]

22. Bolden JE, Peart MJ, Johnstone RW. Anticancer activities of histone deacetylase inhibitors. *Nature reviews Drug discovery* 2006;5(9):769–84 doi 10.1038/nrd2133. [PubMed: 16955068]
23. Knutson SK, Warholic NM, Wigle TJ, Klaus CR, Allain CJ, Raimondi A, et al. Durable tumor regression in genetically altered malignant rhabdoid tumors by inhibition of methyltransferase EZH2. *Proc Natl Acad Sci U S A* 2013;110(19):7922–7 doi 10.1073/pnas.1303800110. [PubMed: 23620515]
24. Arts J, King P, Marien A, Floren W, Belien A, Janssen L, et al. JNJ-26481585, a novel “second-generation” oral histone deacetylase inhibitor, shows broad-spectrum preclinical antitumoral activity. *Clin Cancer Res* 2009;15(22):6841–51 doi 10.1158/1078-0432.CCR-09-0547. [PubMed: 19861438]
25. Wang Y, Huang JW, Li M, Cavenee WK, Mitchell PS, Zhou X, et al. MicroRNA-138 modulates DNA damage response by repressing histone H2AX expression. *Mol Cancer Res* 2011;9(8):1100–11 doi 10.1158/1541-7786.MCR-11-0007. [PubMed: 21693595]
26. Hughes CS, McConechy MK, Cochrane DR, Nazeran T, Karnezis AN, Huntsman DG, et al. Quantitative Profiling of Single Formalin Fixed Tumour Sections: proteomics for translational research. *Sci Rep* 2016;6:34949 doi 10.1038/srep34949. [PubMed: 27713570]
27. Suomi T, Corthals GL, Nevalainen OS, Elo LL. Using Peptide-Level Proteomics Data for Detecting Differentially Expressed Proteins. *J Proteome Res* 2015;14(11):4564–70 doi 10.1021/acs.jproteome.5b00363. [PubMed: 26380941]
28. Child F, Ortiz-Romero PL, Alvarez R, Bagot M, Stadler R, Weichenthal M, et al. Phase II multicentre trial of oral quisinostat, a histone deacetylase inhibitor, in patients with previously treated stage IB-IVA mycosis fungoides/Sezary syndrome. *Br J Dermatol* 2016;175(1):80–8 doi 10.1111/bjd.14427. [PubMed: 26836950]
29. Venugopal B, Baird R, Kristeleit RS, Plummer R, Cowan R, Stewart A, et al. A phase I study of quisinostat (JNJ-26481585), an oral hydroxamate histone deacetylase inhibitor with evidence of target modulation and antitumor activity, in patients with advanced solid tumors. *Clin Cancer Res* 2013;19(15):4262–72 doi 10.1158/1078-0432.CCR-13-0312. [PubMed: 23741066]
30. Rosson GB, Bartlett C, Reed W, Weissman BE. BRG1 loss in MiaPaCa2 cells induces an altered cellular morphology and disruption in the organization of the actin cytoskeleton. *J Cell Physiol* 2005;205(2):286–94 doi 10.1002/jcp.20397. [PubMed: 15887247]
31. Telles E, Seto E. Modulation of cell cycle regulators by HDACs. *Front Biosci (Schol Ed)* 2012;4:831–9. [PubMed: 22202094]
32. Nagl NG, Jr., Zweitzig DR, Thimmapaya B, Beck GR, Jr. Moran E The c-myc gene is a direct target of mammalian SWI/SNF-related complexes during differentiation-associated cell cycle arrest. *Cancer Res* 2006;66(3):1289–93 doi 10.1158/0008-5472.CAN-05-3427. [PubMed: 16452181]
33. van der Vlag J, Otte AP. Transcriptional repression mediated by the human polycomb-group protein EED involves histone deacetylation. *Nat Genet* 1999;23(4):474–8 doi 10.1038/70602. [PubMed: 10581039]
34. Kim HJ, Bae SC. Histone deacetylase inhibitors: molecular mechanisms of action and clinical trials as anti-cancer drugs. *American journal of translational research* 2011;3(2):166–79. [PubMed: 21416059]
35. Muscat A, Popovski D, Jayasekara WS, Rossello FJ, Ferguson M, Marini KD, et al. Low-Dose Histone Deacetylase Inhibitor Treatment Leads to Tumor Growth Arrest and Multi-Lineage Differentiation of Malignant Rhabdoid Tumors. *Clin Cancer Res* 2016;22(14):3560–70 doi 10.1158/1078-0432.CCR-15-2260. [PubMed: 26920892]
36. Wilson BG, Wang X, Shen X, McKenna ES, Lemieux ME, Cho YJ, et al. Epigenetic antagonism between polycomb and SWI/SNF complexes during oncogenic transformation. *Cancer Cell* 2010;18(4):316–28 doi 10.1016/j.ccr.2010.09.006. [PubMed: 20951942]
37. Yamaguchi J, Sasaki M, Sato Y, Itatsu K, Harada K, Zen Y, et al. Histone deacetylase inhibitor (SAHA) and repression of EZH2 synergistically inhibit proliferation of gallbladder carcinoma. *Cancer Sci* 2010;101(2):355–62 doi 10.1111/j.1349-7006.2009.01387.x. [PubMed: 19860841]

38. Takashina T, Kinoshita I, Kikuchi J, Shimizu Y, Sakakibara-Konishi J, Oizumi S, et al. Combined inhibition of EZH2 and histone deacetylases as a potential epigenetic therapy for non-small-cell lung cancer cells. *Cancer Sci* 2016;107(7):955–62 doi 10.1111/cas.12957. [PubMed: 27116120]
39. Fiskus W, Wang Y, Sreekumar A, Buckley KM, Shi H, Jillella A, et al. Combined epigenetic therapy with the histone methyltransferase EZH2 inhibitor 3-deazaneplanocin A and the histone deacetylase inhibitor panobinostat against human AML cells. *Blood* 2009;114(13):2733–43 doi 10.1182/blood-2009-03-213496. [PubMed: 19638619]
40. Knutson SK, Kawano S, Minoshima Y, Warholic NM, Huang KC, Xiao Y, et al. Selective inhibition of EZH2 by EPZ-6438 leads to potent antitumor activity in EZH2-mutant non-Hodgkin lymphoma. *Mol Cancer Ther* 2014;13(4):842–54 doi 10.1158/1535-7163.MCT-13-0773. [PubMed: 24563539]
41. Laporte AN, Barrott JJ, Yao RJ, Poulin NM, Brodin BA, Jones KB, et al. HDAC and Proteasome Inhibitors Synergize to Activate Pro-Apoptotic Factors in Synovial Sarcoma. *PLoS One* 2017;12(1):e0169407 doi 10.1371/journal.pone.0169407. [PubMed: 28056055]
42. Jamshidi F, Bashashati A, Shumansky K, Dickson B, Gokgoz N, Wunder JS, et al. The genomic landscape of epithelioid sarcoma cell lines and tumours. *J Pathol* 2016;238(1):63–73 doi 10.1002/path.4636. [PubMed: 26365879]
43. Karnezis AN, Hoang LN, Coatham M, Ravn S, Almadani N, Tessier-Cloutier B, et al. Loss of switch/sucrose non-fermenting complex protein expression is associated with dedifferentiation in endometrial carcinomas. *Mod Pathol* 2016;29(3):302–14 doi 10.1038/modpathol.2015.155. [PubMed: 26743474]
44. Sauter JL, Graham RP, Larsen BT, Jenkins SM, Roden AC, Boland JM. SMARCA4-deficient thoracic sarcoma: a distinctive clinicopathological entity with undifferentiated rhabdoid morphology and aggressive behavior. *Mod Pathol* 2017 doi 10.1038/modpathol.2017.61.
45. Yoshida A, Kobayashi E, Kubo T, Kodaira M, Motoi T, Motoi N, et al. Clinicopathological and molecular characterization of SMARCA4-deficient thoracic sarcomas with comparison to potentially related entities. *Mod Pathol* 2017;30(6):797–809 doi 10.1038/modpathol.2017.11. [PubMed: 28256572]

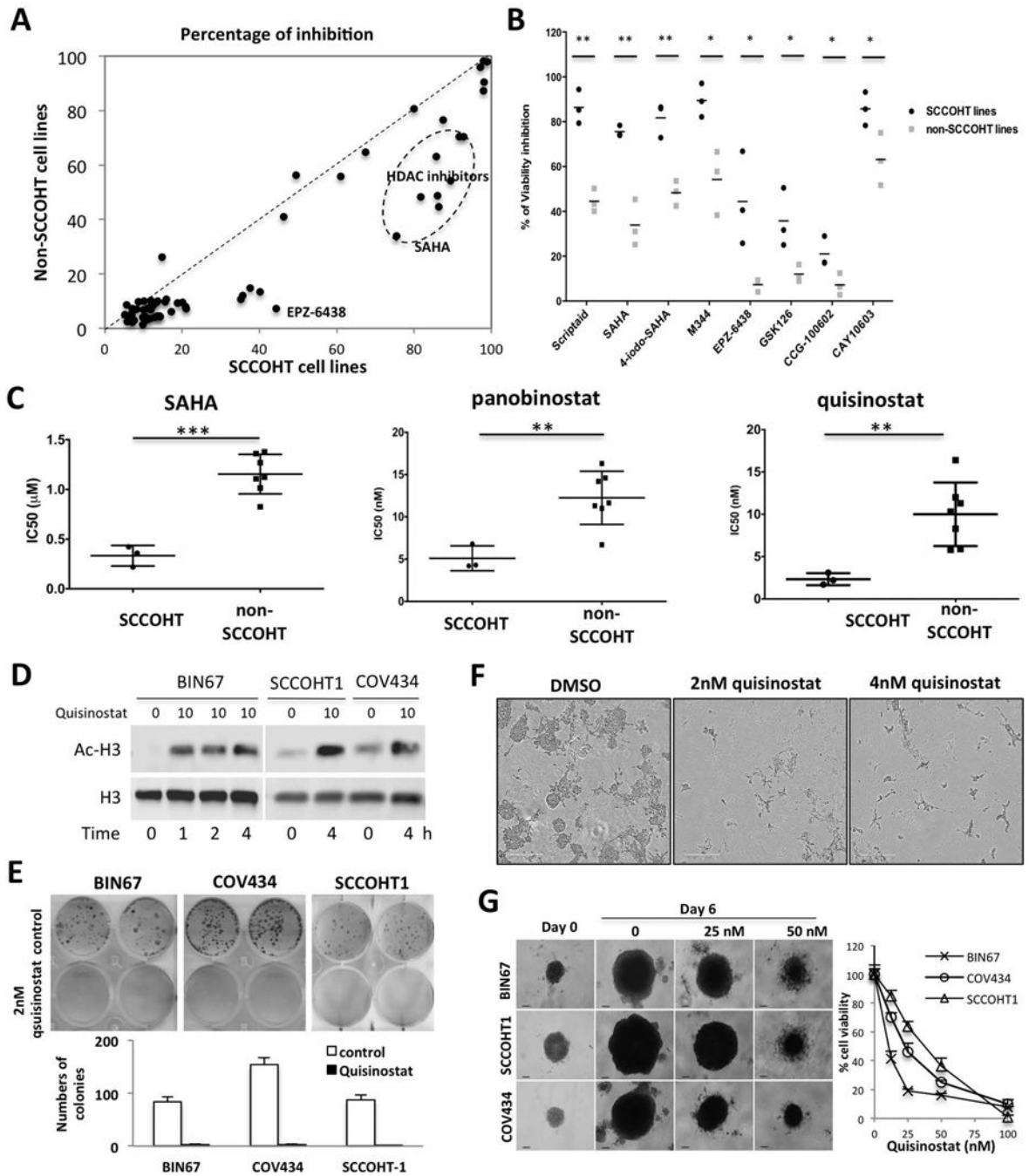


Figure 1. SCCOHT cells are sensitive to HDAC inhibition.

(A) Epigenetic drug screen identifies putative therapeutic agents for SCCOHT. Averaged growth inhibition rates of SCCOHT cell lines by individual drug treatment were plotted against that of the other ovarian cell lines. (B) Epigenetic drugs preferentially suppressed the growth of SCCOHT cells vs other cell lines in the drug screen. (C) SCCOHT cells displayed significantly higher cellular sensitivity to pan-HDAC inhibitors SAHA, panobinostat and quisinostat. Cells were treated with HDAC inhibitors at various doses for 6-days before being fixed and quantitated by crystal violet assay. (D) Quisinostat increased histone H3

acetylation rapidly. (E) Quisinostat suppressed the colony formation ability of SCCOHT cells after two weeks. (F) Quisinostat blocked the formation of spheroids in BIN67 cells. Cells were exposed to quisinostat at indicated doses for 7 days immediately after being embedded in matrigel. (G) Quisinostat inhibited the growth of pre-formed SCCOHT spheroids as measured by Celltiter Glo viability assay. * $P<0.05$, ** $P<0.01$, *** $P<0.001$

Author Manuscript

Author Manuscript

Author Manuscript

Author Manuscript

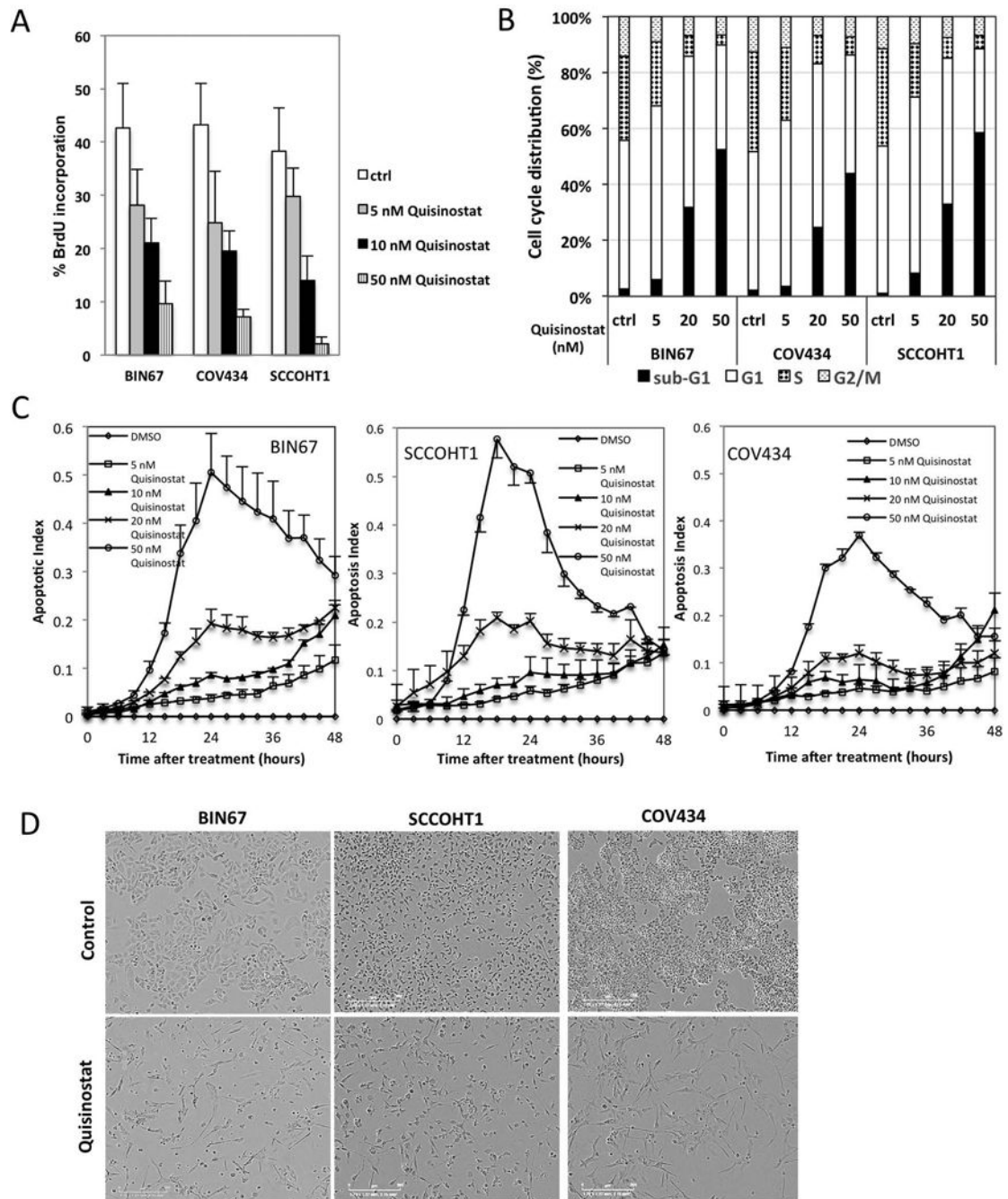


Figure 2. Quisinostat induces cell cycle arrest, apoptosis and differentiation in SCCOHT cells. (A) Quisinostat suppressed SCCOHT cell proliferation as measured by BrdU incorporation after 72 hours of treatment. (B) SCCOHT cell cycle distribution was determined upon quisinostat treatment for 72 hours. (C) Cell apoptosis were quantitated by quantitating caspase3/7 activation through fluorescent microscope coupled with live cell imaging (see Materials and Methods for details) in SCCOHT cells treated with quisinostat. (D) Quisinostat treatment triggered differentiation of SCCOHT cells. Phase contrast images were taken 72 hours after 50 nM quisinostat treatment. * $P < 0.05$, ** $P < 0.01$, *** $P < 0.001$

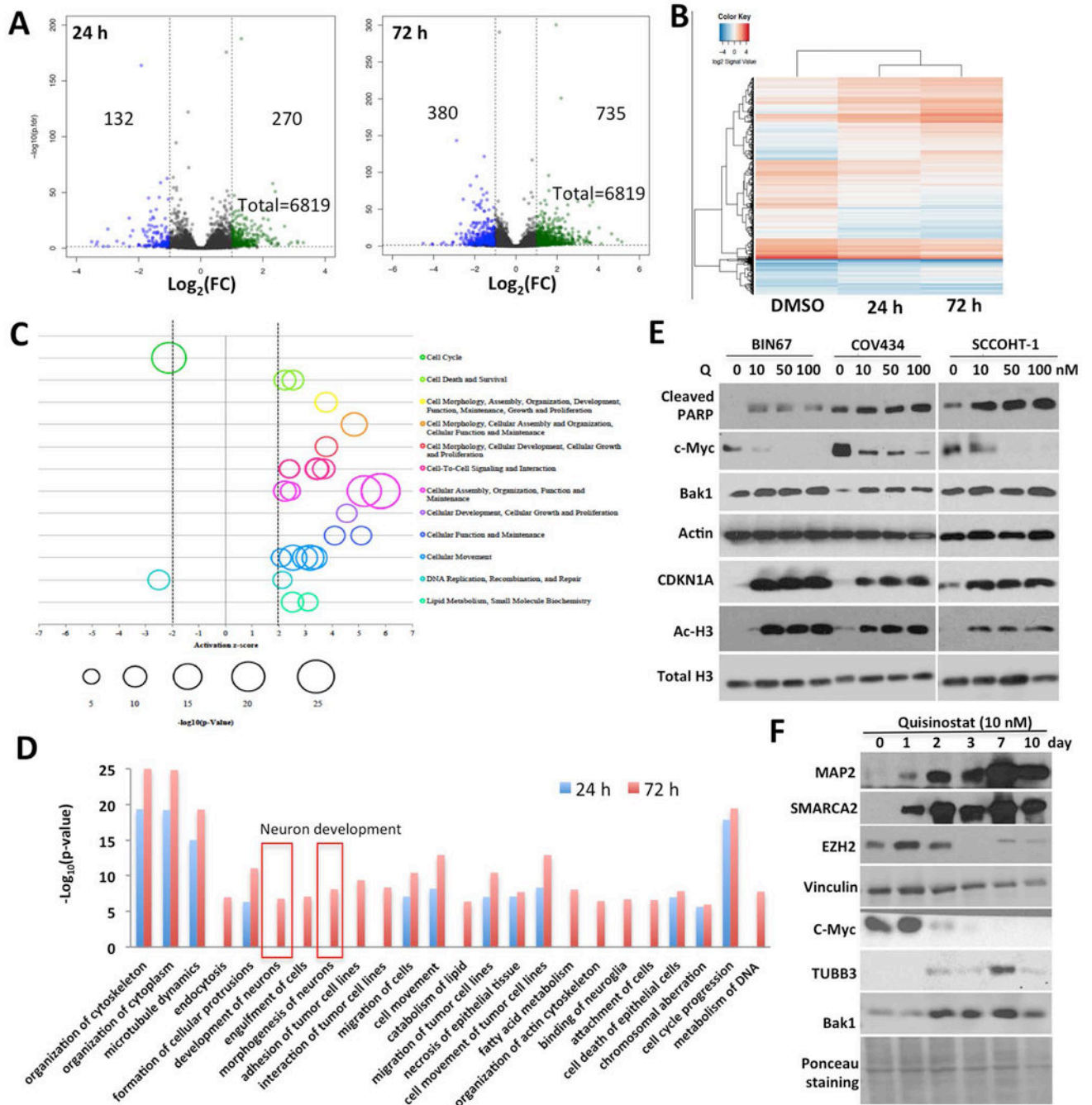


Figure 3. The effect of quisinostat on the proteome of BIN67 cells.

(A) Volcano plot of the proteome of BIN67 cells exposed to 10 nM of quisinostat for 24 or 72 hours in comparison to vehicle treatment. Peptide data were subjected to PECA analysis for identification of significantly altered proteins ($p.fdr < 0.05$ and $|\text{Log}_2\text{FC}| \geq 1$). (B) Clustering analysis of proteins significantly altered by quisinostat treatment for 24 and 72 hours. (C) The enriched biological functions were predicted by IPA analysis of significantly altered proteins caused by quisinostat treatment for 72 hours. (D) Significantly increased ($z\text{-score} > 2$) or decreased ($z\text{-score} < -2$) biological functions were predicted by IPA analysis

upon quisinostat treatment. (E) The expression of cdk inhibitor CDKN1A and apoptotic proteins were induced upon quisinostat treatment for 24 hours by western blot analysis. (F) The expression of SMARCA2, neuronal markers (MAP2, TUBB3) and stem cell markers (EZH2, c-Myc) were analyzed by western blotting in BIN67 cells treated with 10 nM of quisinostat.

Author Manuscript

Author Manuscript

Author Manuscript

Author Manuscript

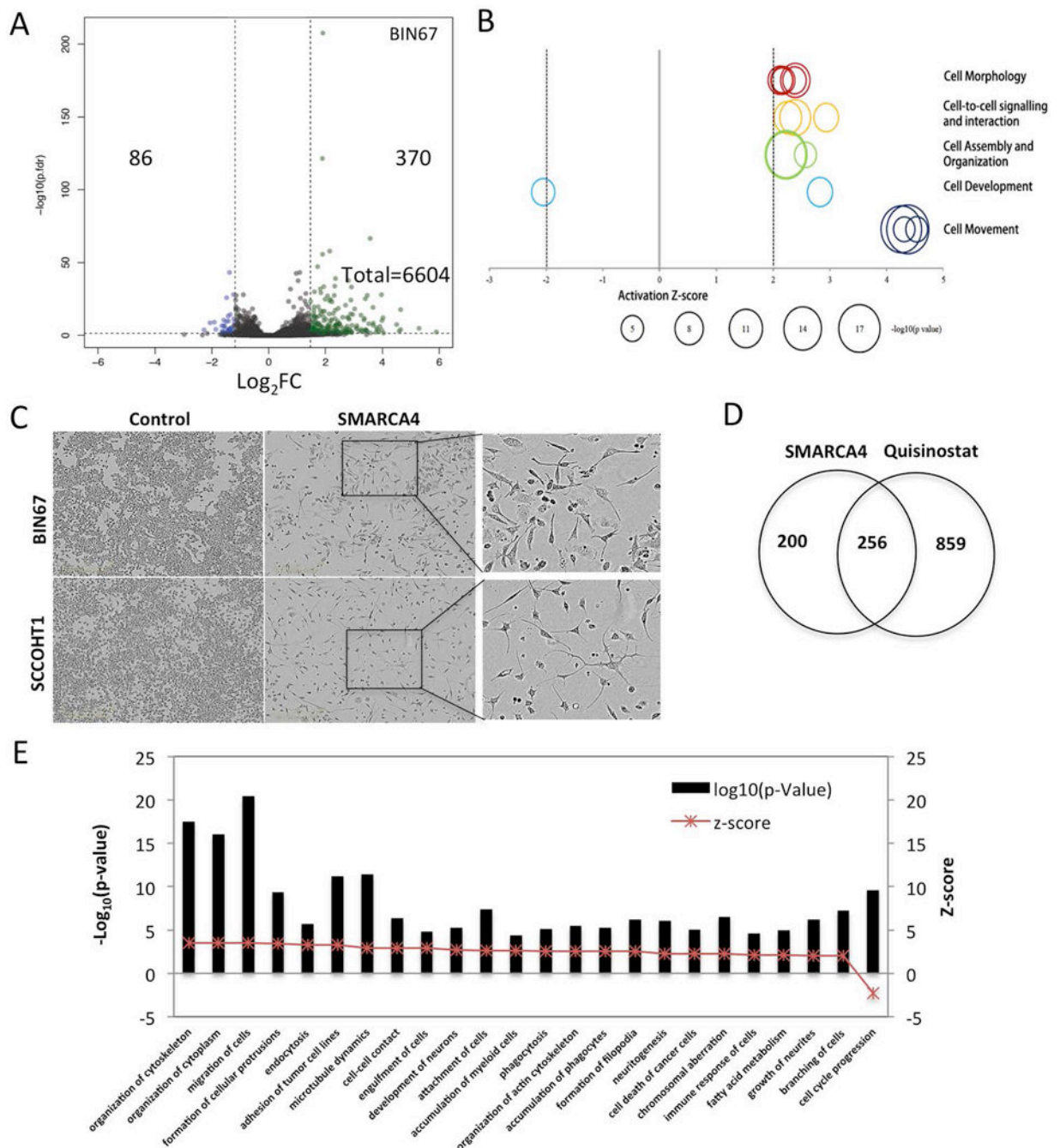


Figure 4. Re-instatement of SMARCA4 mimics the effect of HDAC inhibitors in SCCOHT cells through regulating genes involved in cell fate determination.

(A) Volcano plot of the proteome of BIN67 cells that transduced with GFP or SMARCA4 expressing lentivirus for 96 hours. Peptide data were subjected to PECA analysis for identification of significantly altered proteins ($p.fdr < 0.05$ and $|\text{Log}_2\text{FC}| \geq 1$). (B) The enriched biological functions were predicted by IPA analysis of significantly altered proteins caused by SMARCA4 re-expression. (C) Re-expression of SMARCA4 caused differentiation of SCCOHT cells. (D) SMARCA4 re-expression and quisinostat treatment regulated a common set of proteins. (E) Proteins co-regulated by SMARCA4 and quisinostat were

predicted to significantly activate several biological processes, such as neuritogenesis and decrease cell cycle progression.

Author Manuscript

Author Manuscript

Author Manuscript

Author Manuscript

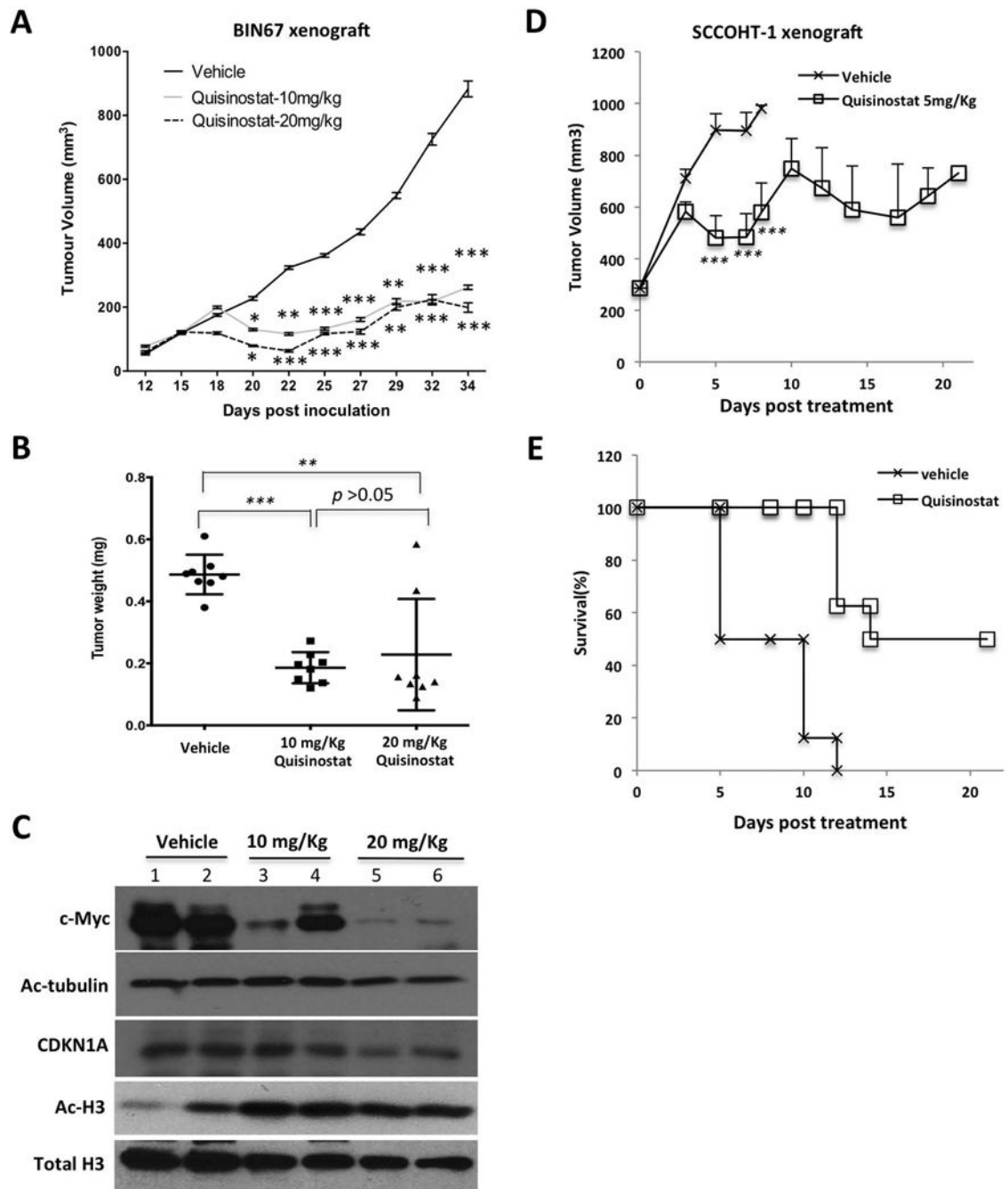


Figure 5. *In vivo* efficacy of quisinostat in SCCOHT mouse xenograft models.

(A-C) The efficacy of quisinostat was evaluated in BIN67-derived mouse subcutaneous xenograft model. Average tumor volumes of either vehicle, 10 or 20 mg/kg quisinostat-treated group were plotted against the time post cell inoculation (A). Final tumor weight was determined and compared between treated groups (B). The effect of quisinostat on downstream targets were evaluated by western blotting for tumors harvested at the end of the study (C). (D, E) Quisinostat suppressed the growth of SCCOHT-1 mouse subcutaneous

xenograft tumors and increased survival of mice to humane endpoint. * $P < 0.05$, ** $P < 0.01$,
*** $P < 0.001$

Author Manuscript

Author Manuscript

Author Manuscript

Author Manuscript

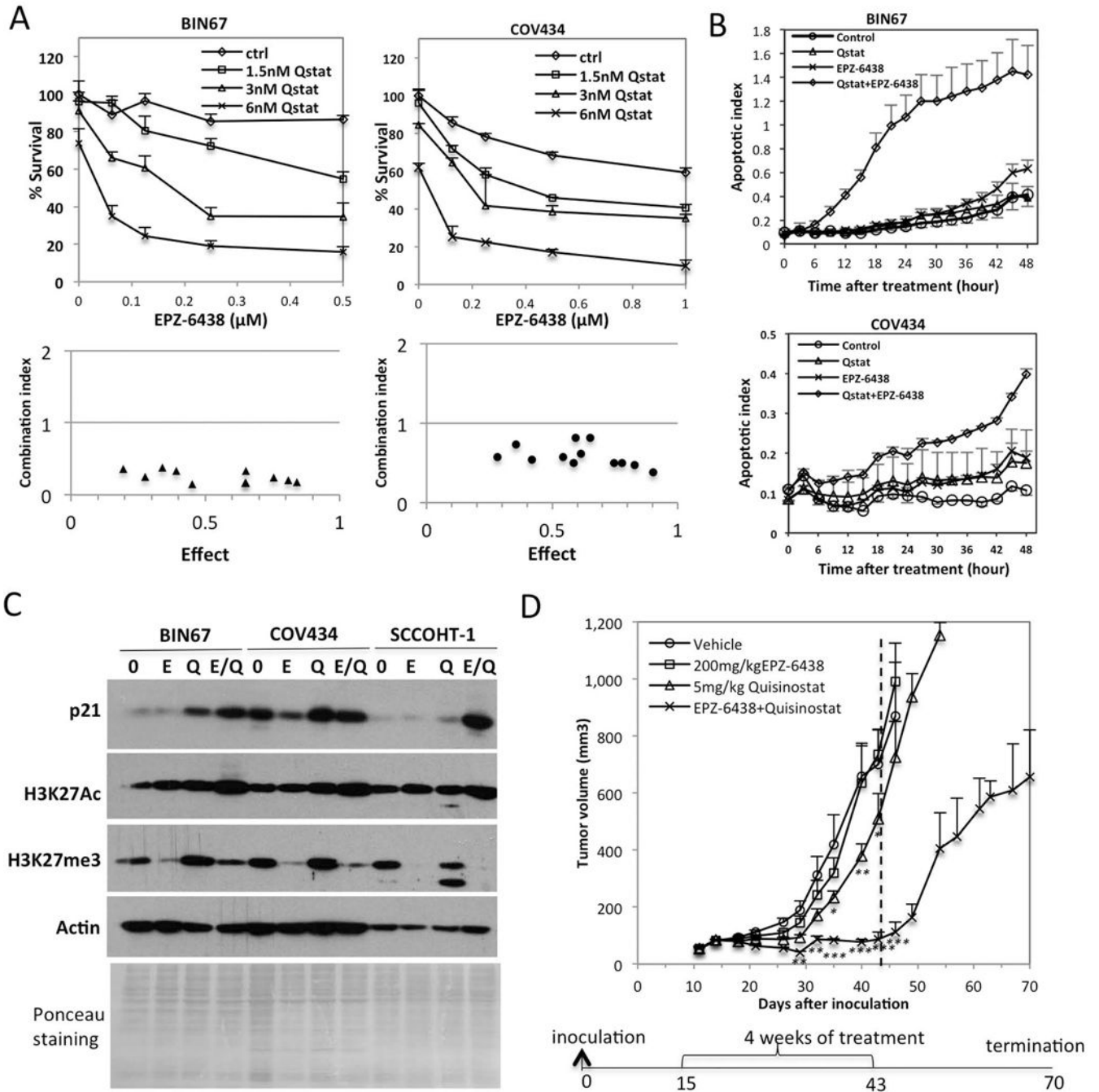


Figure 6. Synergism between quisinostat and EZH2 inhibitor EPZ-6438 in SCCOHT cells.

(A) SCCOHT cells were exposed to combination of quisinostat and EPZ-6438 treatment at various ratio for 6 days and then processed to cell viability measurement by crystal violet assay. Combination index of drugs were calculated using the Chou-Talalay method and the CalcuSyn software. Synergism were predicted when combination index < 1 at each drug combination. (B) Cells were pre-treated with DMSO or $0.25 \mu\text{M}$ EPZ-6438 for 3 days. A cell-permeable apoptosis dye (NucView™ 488 dye) was then added together with or without 2.5 nM quisinostat for monitoring induction of apoptosis. Fluorescent objects were counted

for determination of apoptotic index as described in Materials and Methods. (C) Western blot analysis of histone H3K27 acetylation or tri-methylation levels and CDKN1A expression upon 10 nM quisinostat (Q), 0.5 μ M EPZ-6438 (E) treatment alone or in combination. (D) The *in vivo* efficacy of quisinostat and EPZ-6438 drug combination in the BIN67 xenograft model. Average tumor volumes of each treatment arm were plotted against the time post cell inoculation. * $P < 0.05$, ** $P < 0.01$, *** $P < 0.001$

Author Manuscript

Author Manuscript

Author Manuscript

Author Manuscript